Applied Physics Letters

Perfect optical coherence lattices

Cite as: Appl. Phys. Lett. **119**, 131109 (2021); https://doi.org/10.1063/5.0062924
Submitted: 09 July 2021 . Accepted: 16 September 2021 . Published Online: 30 September 2021

Chunhao Liang, Xin Liu, Zhiheng Xu, et al.

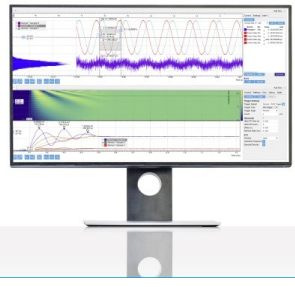

AIP Publishing

Applied Physics Letters ARTICLE scitation.org/journal/apl

Perfect optical coherence lattices

Cite as: Appl. Phys. Lett. **119**, 131109 (2021); doi: 10.1063/5.0062924
Submitted: 9 July 2021 · Accepted: 16 September 2021 ·
Published Online: 30 September 2021

Chunhao Liang,[1,2] Xin Liu,[1,2] Zhiheng Xu,[1,2] Fei Wang,[3,a)] Wei Wen,[4,a)] Sergey A. Ponomarenko,[5,6] Yangjian Cai,[1,2,3,a)] and Pujuan Ma[1,2,a)]

AFFILIATIONS

[1]Shandong Provincial Engineering and Technical Center of Light Manipulation and Shandong Provincial Key Laboratory of Optics and Photonic Devices, School of Physics and Electronics, Shandong Normal University, Jinan 250014, China
[2]Collaborative Innovation Center of Light Manipulations and Applications, Shandong Normal University, Jinan 250358, China
[3]School of Physical Science and Technology, Soochow University, Suzhou 215006, China
[4]College of Mathematics and Physics Science, Hunan University of Arts and Science, Changde 415000, China
[5]Department of Electrical and Computer Engineering, Dalhousie University, Halifax, Nova Scotia B3J 2X4, Canada
[6]Department of Physics and Atmospheric Science, Dalhousie University, Halifax, Nova Scotia B3H 4R2, Canada

[a)]**Authors to whom correspondence should be addressed:** fwang@suda.edu.cn; csuwenwei@126.com; yangjiancai@suda.edu.cn; and pujuanma@foxmail.com

ABSTRACT

We advance and experimentally implement a protocol to generate optical coherence lattices (OCLs) that are not modulated by an envelope field. Here, we dub them perfect OCLs. Structuring the amplitude and phase of an input partially coherent beam in a Fourier plane of an imaging system lies at the heart of our protocol. In the proposed approach, the OCL node profile depends solely on the degree of coherence of the input beam such that, in principle, any lattice structure can be attained via proper manipulations in the Fourier plane. Moreover, any genuine partially coherent source can serve as an input to our lattice generating imaging system. Our results are anticipated to find applications to optical field engineering and multi-target probing among others.

Coherent optical lattices, such as periodic structures of optical field amplitude, phase, or polarization, have long been the focus of attention of the optical community due to a wealth of their applications to the subjects as diverse as neutral gas heating,[1] coherent manipulation of cold atoms,[2] cold-atom superfluidity exploration,[3] and quantum-state control,[4] to mention but a few examples. Recently, optical coherence lattices (OCLs), as an altogether different kind of optical lattices, refer to partially coherent light sources with spatially periodic degrees of coherence.[5] They have triggered much interest ever since their theoretical introduction[5,6] and subsequent exploration.[7–12] OCLs have recently attracted much interest due to their intriguing propagation characteristics. For instance, the periodicity reciprocity arises between the source coherence and far-zone intensity of OCLs on their free space propagation.[6] It has inspired researchers to realize scalar/vector beam arrays with adjustable spatial distributions and node profiles in the far zone or a focal plane of an imaging system.[7–9,11] The propagation of OCLs through the atmospheric and oceanic turbulence has been studied as well. It was found that the OCLs of higher beam order are less distorted by the turbulence than are the conventional Gaussian Schell-model (GSM) beams.[13,14]

Yet, only a few protocols for the experimental realization of OCLs have been reported to date.[15,16] In Ref. 15, an uncorrelated superposition of elementary beams has been utilized to generate OCLs. However, a finite spot size of an elementary beam led to the appearance of an envelope field $J_1(r)/r$ modulating OCLs produced via this protocol. In Ref. 16, OCLs were generated through scattering of a light beam by a specially designed random medium, which imposed envelope fields on the produced OCLs as well. Hence, the inevitability of the envelope field is germane to all the methods for OCLs generation reported in the literature to date. Moreover, although OCLs of different lattice structures can be generated by the protocols of Refs. 15 and 16, these protocols lack simultaneous control of the lattice node profile and the lattice structure.

In this Letter, we draw on a previously elaborated arsenal of Fourier optics techniques to engineer partially coherent beams[17–26] to advance an efficient protocol to realize OCLs. Such beams are not embedded into any envelope field, thereby maintaining a strictly periodic coherence structure that we dub a perfect optical coherence lattice. In our protocol, each OCL node profile depends only on the degree of coherence (DOC) of a light source, and the lattice structure

is determined by the Fourier spectrum of a transmission function of our imaging system. We illustrate our protocol with numerical examples and implement it experimentally.

We start by illustrating in Fig. 1, a typical 4f optical system consisting of two identical thin lenses of focal length f. We place a plate with a complex transmission function $P(\xi)$ at the rear focal plane of lens L1. We treat the front focal plane of lens L1 and the rear focal plane of lens L2 as the input and output planes to our imaging system, respectively. We generate perfect OCLs in the output plane through modulation of the amplitude and phase of an optical beam in the Fourier plane of the system.

We assume the input to our system to be a quasi-monochromatic, statistically stationary beam propagating along the z direction. In the space-frequency domain, the second-order statistics of the beam are characterized by the cross-spectral density (CSD) function $W(\mathbf{r}_1, \mathbf{r}_2, \omega) = \langle E^*(\mathbf{r}_1, \omega) E(\mathbf{r}_2, \omega) \rangle$, where E stands for the random electric field; $\mathbf{r_1}$ and $\mathbf{r_2}$ are two position vectors in the input plane; and the asterisk and the angle brackets denote a complex conjugate and ensemble average, respectively. Furthermore, ω is a frequency of light, which will be omitted hereafter for brevity. As our imaging system is linear, the input and output CSDs are related through a linear transform as

$$W^{(\mathrm{out})}(\mathbf{r}_1', \mathbf{r}_2') = \int W^{(\mathrm{in})}(\mathbf{r}_1, \mathbf{r}_2) h^*(\mathbf{r}_1, \mathbf{r}_1') h(\mathbf{r}_2, \mathbf{r}_2') d^2\mathbf{r}_1 d^2\mathbf{r}_2, \quad (1)$$

where $W^{(\mathrm{in})}$ and $W^{(\mathrm{out})}$ are the input and output CSDs, respectively, $\mathbf{r}_i' = (x_i', y_i')$, $i = 1, 2$ is an arbitrary position vector in the output plane, and $h(\mathbf{r}, \mathbf{r}')$ is a response function of the optical system. For a 4f optical system shown in Fig. 1, the latter takes the form[19]

$$h(\mathbf{r}, \mathbf{r}') = -\frac{1}{\lambda^2 f^2} \int P(\xi) \exp\left[-\frac{ik}{f} \xi \cdot (\mathbf{r} - \mathbf{r}')\right] d^2\xi. \quad (2)$$

Here, ξ is a transverse position vector in the Fourier plane. Equation (2) indicates that the translationally invariant response function is just a Fourier transform of the complex transmission function P. It follows that $h(\mathbf{r}, \mathbf{r}') = h(\mathbf{r} - \mathbf{r}') = \tilde{P}(\mathbf{r} - \mathbf{r}')$, where the tilde denotes the Fourier transform.

On combining Eqs. (1) and (2), we obtain the expression

$$W^{(\mathrm{out})}(\mathbf{r}_1', \mathbf{r}_2') = W^{(\mathrm{in})}(\mathbf{r}_1', \mathbf{r}_2') \otimes h^*(-\mathbf{r}_1') \otimes h(-\mathbf{r}_2'), \quad (3)$$

where $\otimes$ denotes a convolution. To realize perfect OCLs in the output plane, we require the response function of the form

$$h(\mathbf{r} - \mathbf{r}') = -\sum_{m=1}^{M} \delta(x - x' + ma) \delta(y - y' + mb), \quad (4)$$

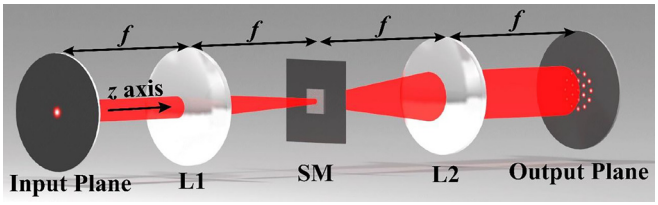

FIG. 1. Schematic diagram of an optical system with Fourier phase lattices. L1 and L2, thin lens; SM, spectral modulator.

where $\delta(\cdot)$ is a Dirac delta function; and a and b are lattice periods along two mutually orthogonal directions that we take to be the x- and y-axes of the Cartesian coordinate system, respectively. On substituting Eq. (4) into Eq. (3) and following the basic property of the Dirac function convolution, we obtain

$$W^{(\mathrm{out})}(\mathbf{r}_1', \mathbf{r}_2') = \sum_{m_1=1}^{M} \sum_{m_2=1}^{M} W^{(\mathrm{in})}(x_1' - m_1 a, y_1' - m_1 b, x_2' - m_2 a, y_2' - m_2 b). \quad (5)$$

We stress here that Eq. (5) is approximately valid even if each δ-function in Eq. (4) is replaced by any narrow support function as long as its widths along the two mutually orthogonal directions are much smaller than those of the CSD $[W^{(in)}]$ of the incident beam. The input–output relation of Eq. (5) can be realized in the laboratory to any desired accuracy. We notice that provided the two lattice periods a and b are much larger than the greater of the spot size and coherence width of the incident beam, the cross terms ($m_1 \neq m_2$) in the sums on the right-hand side of Eq. (5) can be dropped, resulting in the expression

$$W^{(\mathrm{out})}(\mathbf{r}_1', \mathbf{r}_2') \approx \sum_{m=1}^{M} W^{(\mathrm{in})}(x_1' - ma, y_1' - mb, x_2' - ma, y_2' - mb). \quad (6)$$

Next, it follows from the DOC definition[27–29] that:

$$\mu^{(\mathrm{out})}(\mathbf{r}_1', \mathbf{r}_2') = \frac{W^{(\mathrm{out})}(\mathbf{r}_1', \mathbf{r}_2')}{\sqrt{I^{(\mathrm{out})}(\mathbf{r}_1')} \sqrt{I^{(\mathrm{out})}(\mathbf{r}_2')}}, \quad (7)$$

where $I^{(\mathrm{out})}(\mathbf{r}') = W^{(\mathrm{out})}(\mathbf{r}', \mathbf{r}')$ is an average output intensity. Notice that the output CSD is a superposition of M non-overlapping terms corresponding to field correlations within M individual nodes of the OCLs. It follows that whenever $\mathbf{r}_1'$ and $\mathbf{r}_2'$ are situated within the nth node of the lattice, the substitution from Eq. (6) into Eq. (7) yields

$$\mu^{(\mathrm{out})}(\mathbf{r}_1', \mathbf{r}_2') \approx \frac{W^{(\mathrm{in})}(x_1' - na, y_1' - nb, x_2' - na, y_2' - nb)}{\sqrt{I^{(in)}(x_1' - na, y_1' - nb)} \sqrt{I^{(\mathrm{in})}(x_2' - na, y_2' - nb)}} = \mu^{(\mathrm{in})}(x_1' - na, y_1' - nb, x_2' - na, y_2' - nb). \quad (8)$$

On the other hand, if $\mathbf{r}_1'$ and $\mathbf{r}_2'$ are located in different individual nodes of the lattice, the output field is completely uncorrelated at these pairs of points such that

$$\mu^{(\mathrm{out})}(\mathbf{r}_1', \mathbf{r}_2') = 0. \quad (9)$$

It then follows that, in general,

$$\mu^{(\mathrm{out})}(\mathbf{r}_1', \mathbf{r}_2') \approx \sum_{m=1}^{M} \mu^{(\mathrm{in})}(x_1' - ma, y_1' - mb, x_2' - ma, y_2' - mb). \quad (10)$$

The DOC in Eq. (10) has a functional form of a perfect OCLs: The spatial node profile of the lattice is determined by the DOC of the incident beam, while the function P controls the overall lattice structure. Equation (10) is then the main result of this Letter.

To demonstrate the feasibility of our method, we first perform numerical simulations for a random input beam of the Gaussian intensity and degree of coherence.[27] We choose an input beam width σ_0 and its coherence length δ_0 such that $\sigma_0 = \delta_0 = 0.5$ mm, and the other parameters are: $f = 400$ mm and $\lambda = 632$ nm. Next, we introduce three complex filters to generate three kinds of perfect OCLs. We exhibit the moduli and phase distributions of the corresponding P functions in Figs. 2(a1)–2(c1) and Figs. 2(a2)–2(c2), respectively. In Figs. 2(a3)–2(c3), we show the OCLs numerically generated with the aid of these complex transmission functions. The adjacent nodes of each OCL are separated by the distance of 3 mm. Our simulations indicate that the lattice structure can be easily adjusted by varying the lattice periods. Furthermore, to illustrate the OCL node profile control, we studied three Gaussian input beams with the DOC structure generated by the Hermite–Gaussian correlated Schell-model (HGCSM), the Laguerre–Gaussian correlated Schell-model (LGCSM), and cosine-Gaussian correlated Schell-model (CGCSM) sources. The detailed CSD structure of these sources can be found in Refs. 30–32. As a particular example, we display in Fig. 3 the OCLs numerically generated with these three input beams with the help of the complex transmission function with the amplitude and phase shown in Figs. 2(b1) and 2(b2), respectively. We can infer from Figs. 2 and 3 that the OCL structure and the node profile can be readily controlled by manipulating the input DOC and the complex transmission function of our imaging system.

We now show how perfect OCLs can be realized in the laboratory. Our protocol hinges on the ability to simultaneously modulate the amplitude and phase of the complex transmission function P in the Fourier plane of our imaging system. Here, we adopt encoding the information about the function P into a phase-only spatial light modulator (SLM). As suggested in Refs. 34–36, the hologram phase that is loaded onto the SLM is specified by

$$\Phi_{\mathrm{SLM}} = A_f \sin\left[Arg(P) + 2\pi f_x x\right], \tag{11}$$

where A_f can be obtained by the numerical inversion of $J_1(A_f) = |P|$. J_1 is the first-order Bessel function of the first kind; f_x denotes a grating frequency. Here, we take Fig. 4(a) as an example to discuss its generation. Figs. 2(a1) and 2(a2) are treated as the amplitude and phase of the function P for the case M = 4. Substituting these amplitude and phase into Eq. (11), we obtain Fig. 4(a). Following the same principle, we generate the holograms shown in Figs. 4(b) and 4(c) for M = 9 and M = 19 cases corresponding to the functions P shown in Figs. 2(b1), 2(b2), 2(c1), and 2(c2), respectively. To this end, we inserted the phase only SLM into the Fourier plane and loaded computer generated phase holograms onto it to implement the encoding.

We sketch our experimental setup in Fig. 5. A He-Ne laser emits a light of the carrier wavelength $\lambda = 632.8$ nm. It arrives at the first spatial light modulator (SLM1) after having been transmitted through a linear polarizer (LP) and a beam splitter (BS). The SLM1 acts as a phase programmable hologram. The beam emerging from the SLM1 and reflected by the BS passes through a thin lens L1 and reaches a rotating ground-glass disk (RGGD). We can employ any hologram to engineer a beam intensity profile on the RGGD. The distance between L1 and RGGD is used to control the coherence width of the beam.[32] Upon transmission through the RGGD, L2, and GAF, a partially coherent input beam with prescribed DOC emerges. The DOC of the emerging beam is given by a Fourier transform of the intensity profile of the beam incident on the RGGD.[32] Next, the generated partially coherent beam is focused by a thin lens L3 and illuminates a predesigned hologram on an SLM2. A positive or negative first-order diffraction pattern is then selected by a circular aperture (CA) and transmitted through a thin lens L4. In the rear focal plane of L4, which

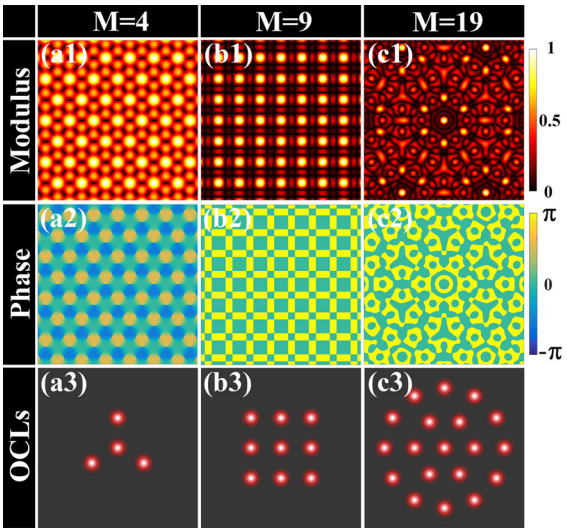

FIG. 2. Simulation results for generation of perfect OCLs $[|\mu^{(\mathrm{out})}(\mathbf{r}_1', \mathbf{r}_2' = 0)|^2]$ of variable lattice structures [(a3)-(c3)] produced via Fourier spectrum modulation. The amplitude and phase distributions of the relevant P functions are displayed in Figs. 2(a1)–2(c1) and Figs. 2(a2)–2(c2), respectively. The input is a Gaussian Schell-model beam. The distance between the adjacent nodes of each lattice in Figs. 2(a3)–2(c3) is 3 mm.

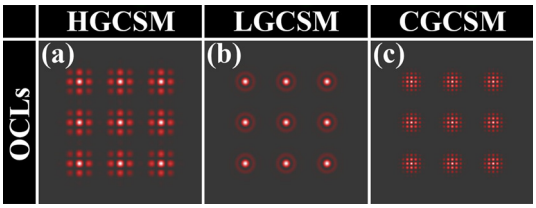

FIG. 3. Simulation results for generation of perfect OCLs $[|\mu^{(\mathrm{out})}(\mathbf{r}_1', \mathbf{r}_2' = 0)|^2]$ of controllable node profiles. Input beams: (a) HGCSM beam with the indices n = m = 2, (b) LGCSM beam of the order n = 4, and (c) CGCSM beam of the order n = 2. The distance between the adjacent nodes of each lattice equals to 3 mm.

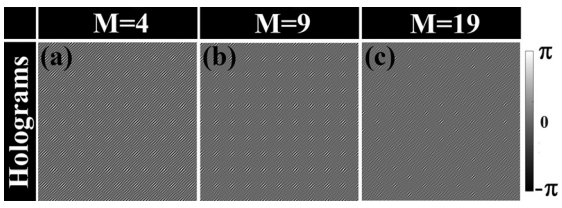

FIG. 4. Computer generated holograms of the complex transmission functions of the imaging system producing prefect OCLs.

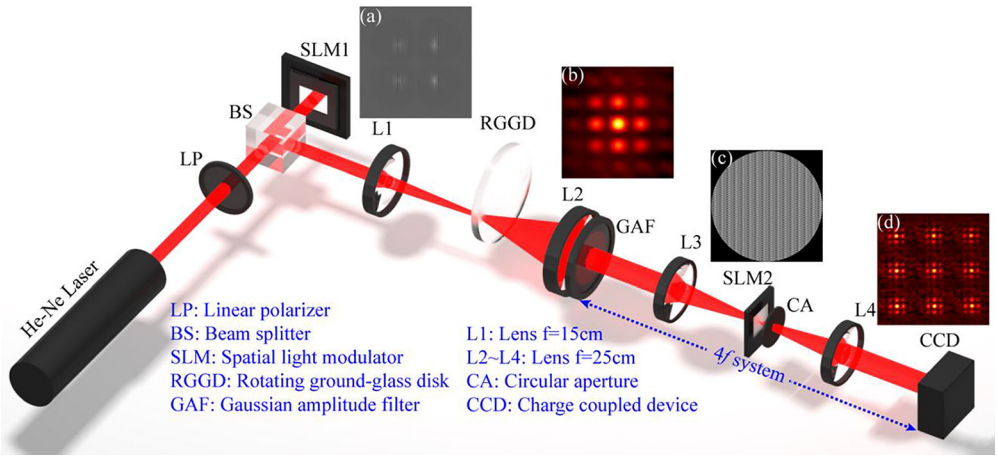

FIG. 5. Experimental setup to generate perfect OCLs. The insets (a)-(d) illustrate the implementation of an OCL with a Hermite–Gaussian node profile. (a) Hologram on the SLM1, (b) DOC distribution of the input beam just past a GAF, (c) hologram on the SLM2, and (d) OCL profile.

serves as the output plane to our imaging system, we place a CCD camera to record the random intensity distribution of an output beam. As the light transmitted through the RGGD obeys Gaussian statistics, the Gaussian moment theorem27 implies that the DOC of the output beam can be expressed in terms of the intensity correlations as

$$|\mu^{(out)}(\mathbf{r}_1', \mathbf{r}_2')|^2 = \frac{\sum_{n=1}^{N} I_n(\mathbf{r}_1') I_n(\mathbf{r}_2')}{N I(\mathbf{r}_1') I(\mathbf{r}_2')} - 1. \quad (12)$$

Here, N is a number of ensemble realizations, $I_n(\mathbf{r}')$ is an intensity of the n-th realization, and $I(\mathbf{r}') = \sum_{n=1}^{N} I_n(\mathbf{r}')/N$ stands for an average intensity over the ensemble, see, cf. Ref. 33 for more details. In our experiment, the beam spot size and the coherence width were measured to be $\sigma_0 = 0.35$ mm and $\delta_0 = 0.17$ mm, respectively, and the number of ensemble realizations was taken to be 5×10^3. On comparing Figs. 3 and 6, we can report good agreement between the experiment and numerical simulations, testifying to the practicality of the proposed protocol of perfect OCLs generation.

In summary, we have introduced the concept of perfect optical coherence lattices and advanced a protocol for their experimental realization. We have verified our protocol with numerical simulations and implemented it experimentally. Our results open new possibilities for generating customizable perfect optical lattices that are anticipated to find applications to beam splitting, multi-target probing, and free-space optical communications. Finally, we discuss the realization of vector optical coherence lattices. First, we can generate a linearly polarized perfect OCL with the help of a polarizer. Such an OCL can then be converted into a uniformly polarized OCL with a circular polarization, say, with the help of a suitably modified Mach–Zehnder interferometer setup. We can also employ a polarization convertor to convert a linearly polarized OCL to a non-uniformly polarized one with a desired polarization state such as radial or azimuthal polarization.

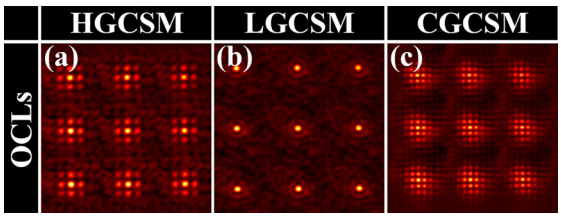

FIG. 6. Experimental results for $|\mu^{(out)}(\mathbf{r}_1', \mathbf{r}_2' = 0)|^2$ of perfect OCLs. The coherence width and the spot size of input partially coherent beams are $\sigma_0 = 0.35$ mm and $\delta_0 = 0.17$ mm, respectively. The distance between the adjacent nodes equals to 0.73 mm.

This work was supported by the National Key Research and Development Program of China (No. 2019YFA0705000), the Local Science and Technology Development Project of the Central Government (No. YDZX20203700001766), the National Natural Science Foundation of China (Nos. 11525418, 11874046, 11947239, 11974218, 91750201, 12004220, and 12004225), the Natural Sciences and Engineering Research Council of Canada (No. RGPIN-2018-05497), the Innovation group of Jinan (No. 2018GXRC010), and the China Postdoctoral Science Foundation (Nos. 2019M662424 and 2020M672112).

DATA AVAILABILITY

The data that support the findings of this study are available from the corresponding authors upon reasonable request.

REFERENCES

[1]B. M. Cornella, S. F. Gimelshein, T. C. Lilly, and A. D. Ketsdever, Appl. Phys. Lett. **103**, 194103 (2013).
[2]Q. Beaufils, G. Tackmann, X. Wang, B. Pelle, S. Pelisson, P. Wolf, and F. P. dos Santos, Phys. Rev. Lett. **106**, 213002 (2011).
[3]J. K. Chin, D. E. Miller, Y. Liu, C. Stan, W. Setiawan, C. Sanner, K. Xu, and W. Ketterle, Nature **443**, 961 (2006).
[4]I. H. Deutsch and P. S. Jessen, Phys. Rev. A **57**, 1972 (1998).
[5]L. Ma and S. A. Ponomarenko, Opt. Lett. **39**, 6656 (2014).
[6]L. Ma and S. A. Ponomarenko, Opt. Express **23**, 1848 (2015).

[7]C. Liang, C. Mi, F. Wang, C. Zhao, Y. Cai, and S. A. Ponomarenko, Opt. Express **25**, 9872 (2017).
[8]C. Liang, X. Zhu, C. Mi, X. Peng, F. Wang, Y. Cai, and S. A. Ponomarenko, Opt. Lett. **43**, 3188 (2018).
[9]S. Zhu, J. Wang, X. Liu, Y. Cai, and Z. Li, Appl. Phys. Lett. **109**, 161904 (2016).
[10]Y. Chen, A. Norrman, S. A. Ponomarenko, and A. T. Friberg, Opt. Lett. **43**, 3429 (2018).
[11]Z. Mei and O. Korotkova, Opt. Lett. **43**, 2676 (2018).
[12]X. Liu, L. Liu, X. Peng, L. Liu, F. Wang, Y. Gao, and Y. Cai, J. Quant. Spectrosc. Radiat. **222–223**, 138 (2019).
[13]X. Liu, J. Yu, Y. Cai, and S. A. Ponomarenko, Opt. Lett. **41**, 4182 (2016).
[14]X. Huang, Z. Deng, X. Shi, Y. Bai, and X. Fu, Opt. Express **26**, 4786 (2018).
[15]Y. Chen, S. A. Ponomarenko, and Y. Cai, Appl. Phys. Lett. **109**, 061107 (2016).
[16]Y. Ding and D. Zhao, Opt. Express **25**, 25222 (2017).
[17]T. Wu, C. Liang, F. Wang, and Y. Cai, J. Opt. **19**, 124010 (2017).
[18]C. Mi, C. Liang, F. Wang, L. Liu, Y. Gao, and Y. Cai, J. Quant. Spectrosc. Radiat **222–223**, 145 (2019).
[19]X. Liu, D. Xia, Y. E. Monfared, C. Liang, F. Wang, Y. Cai, and P. Ma, Opt. Express **28**, 9777 (2020).
[20]Y. Chen, S. A. Ponomarenko, and Y. Cai, Sci. Rep. **7**, 39957 (2017).
[21]H. Mao, Y. Chen, C. Liang, L. Chen, Y. Cai, and S. A. Ponomarenko, Opt. Express **27**(10), 14353 (2019).
[22]X. Zhao, T. D. Visser, and G. P. Agrawal, Opt. Lett. **43**, 2344 (2018).
[23]T. D. Visser, G. P. Agrawal, and P. W. Milonni, Opt. Lett. **42**(22), 4600–4602 (2017).
[24]Y. Shen, H. Sun, D. Peng, Y. Chen, Q. Cai, D. Wu, F. Wang, Y. Cai, and S. A. Ponomarenko, Appl. Phys. Lett. **118**, 181102 (2021).
[25]D. Peng, Z. Huang, Y. Liu, Y. Chen, F. Wang, S. A. Ponomarenko, and Y. Cai, PhotoniX **2**, 6 (2021).
[26]X. Lu, Y. Shao, C. Zhao, S. Konijnenberg, X. Zhu, Y. Tang, Y. Cai, and H. P. Urbach, Adv. Photonics **1**, 016005 (2019).
[27]L. Mandel and E. Wolf, *Optical Coherence and Quantum Optics* (Cambridge University Press, 1995).
[28]S. A. Ponomarenko and E. Wolf, Opt. Commun. **170**, 1 (1999).
[29]S. A. Ponomarenko and E. Wolf, Opt. Commun. **227**, 73 (2003).
[30]Y. Chen, J. Gu, F. Wang, and Y. Cai, Phys. Rev. A **91**, 013823 (2015).
[31]Z. Mei and O. Korotkova, Opt. Lett. **38**, 91 (2013).
[32]C. Liang, F. Wang, X. Liu, Y. Cai, and O. Korotkova, Opt. Lett. **39**, 769 (2014).
[33]P. Ma, B. Kacerovská, R. Khosravi, C. Liang, J. Zeng, X. Peng, C. Mi, Y. E. Monfared, Y. Zhang, F. Wang, and Y. Cai, Appl. Sci. **9**, 2084 (2019).
[34]C. Rosales-Guzmán and A. Forbes, *How to Shape Light with Spatial Light Modulators* (SPIE, 2017).
[35]E. Bolduc, N. Bent, E. Santamato, E. Karimi, and R. W. Boyd, Opt. Lett. **38**, 3546 (2013).
[36]X. Liu, Y. E. Monfared, R. Pan, P. Ma, Y. Cai, and C. Liang, Appl. Phys. Lett. **119**, 021105 (2021).